Enhanced water permeability and osmotic power generation with sulfonate-functionalized porous polymer-incorporated thin film nanocomposite membranes

Ralph Rolly Gonzales[a#], *Yanqin Yang*[b#], *Myoung Jun Park*[a], *Tae-Hyun Bae*[c], *Ahmed Abdel-Wahab*[d], *Sherub Phuntsho*[a], *Ho Kyong Shon*[a,*]

[a]Centre for Technology in Water and Wastewater, University of Technology Sydney, New South Wales, Australia

[b]National-Local Joint Engineering Laboratory for Energy Conservation in Chemical Process Integration and Resources Utilization, School of Chemical Engineering and Technology, Hebei University of Technology, Tianjin, China

[c]Department of Chemical and Biomolecular Engineering, Korea Advanced Institute of Science and Technology, Daejeon, South Korea

[d]Chemical Engineering Program, Texas A & M University at Qatar, Education City, Doha, Qatar

[#]These authors contributed equally to this work.

[*]Corresponding author: Ho Kyong Shon; Email: hokyong.shon-1@uts.edu.au

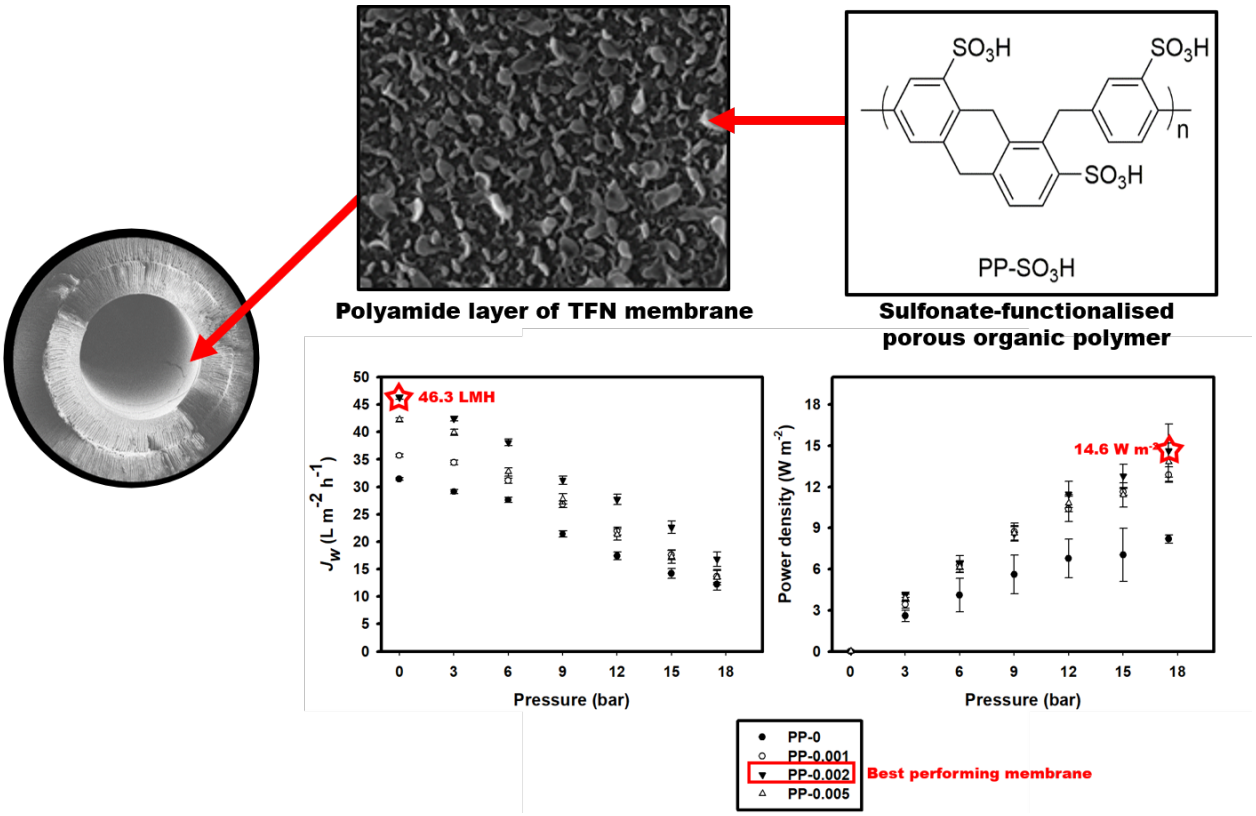
Polyamide layer of TFN membrane
Sulfonate-functionalised porous organic polymer
PP-SO3H
46.3 LMH
14.6 W m-2
Pressure (bar)
Pressure (bar)
PP-0
PP-0.001
PP-0.002
PP-0.005
Best performing membrane

16

ABSTRACT

In this study, a hydrophobic porous organic polymer (PP) synthesized via *Friedel-Crafts* alkylation of dichloro-*p*-xylene, was functionalized with hydrophilic sulfonate functional group to form PP-SO_3H, prior to incorporation into the polyamide layer of a hollow fiber pressure retarded osmosis (PRO) TFN membrane. Sulfonate functionalization of the PP material improved the compatibility of the nanomaterial with the aqueous amine precursor during the *in situ* interfacial polymerization, leading to a decrease in aggregation of the nanoparticles. The effect of nanomaterial loading on the membranes' performance was also elucidated. PP-SO_3H incorporation resulted in significant improvement of surface hydrophilicity, which along with improved porosity, facilitated enhanced water transport across the membrane and maintained an acceptable salt rejection of the selective layer. The best-performing membrane with PP-SO_3H loading of 0.002 wt. % showed a 46.3 L m^{-2} h^{-1} water flux and power density of 14.6 W m^{-2}, which are both the highest values recorded. This study suggests that the functionality and chemical properties of the nanomaterial in a TFN membrane is essential in improving altogether the osmotic performance and salinity gradient power harvesting capability during PRO.

KEYWORDS

Pressure retarded osmosis; Membrane; Thin film nanocomposite; Porous polymer; Sulfonate functional group

INTRODUCTION

There has been an increase recently in the demand for new sustainable renewable energy sources due to the impending depletion of fossil fuels and their adverse contribution to global warming and subsequent climate change. The interest in sustainable renewable energy leads to the development and continuous research on alternative sources like solar, wind, biomass, geothermal sources, and osmotic energy [1-3]. Osmotic energy is one such potential energy source that can be generated from the Gibbs free energy of mixing solutions [1]. Furthermore, industrialization and the exponential increase of the world's population do not only increase the demand for energy, there is also an increased demand for clean, fresh water [4].

Pressure retarded osmosis (PRO), is a process known to have a great potential in renewable energy harvesting by utilizing the concentration and/or osmotic pressure difference between two streams of varying salinity, where water from the low-concentrated feed solution passes through a dense selective membrane towards the direction of the higher-concentrated draw solution by natural osmosis. While largely similar to the forward osmosis (FO) process, hydraulic pressure is applied against the osmotic pressure direction in the PRO process, and while slightly retarding the movement of water towards the draw solution. The spontaneous mixing of the two streams of different salinity leads to the production of free energy of mixing which is then converted into mechanical energy as it passes through a hydro-turbine which then generates electrical energy [5]. Not only can PRO augment the world's need for alternative energy sources, PRO, as an osmotic process, can also be applied for desalination or wastewater reuse, which both can provide solutions to the world's water crisis.

Lack of a suitable semi-permeable membranes solely for PRO process is one of the major challenges in the commercialization of the PRO technology. Ideal PRO membranes must possess

the following properties: high hydrophilicity and porosity to facilitate water flux, high selectivity, low structural parameter (S), and satisfactory mechanical strength to resist hydraulic pressure throughout PRO operation [6]. Typical PRO membranes are made up of a thin film composite (TFC) membranes consisting of a highly porous membrane support layer prepared by polymer non-solvent induced phase inversion (NIPS) method and a dense thin film selective layer formed by polymerization reaction on the interface of the membrane support [7, 8]. While significant progresses have been achieved on PRO membrane development in recent times [9], membrane performance remains limited by issues, such as membrane fouling and internal concentration polarization (ICP). In the PRO process, ICP refers to the concentration increase of the less concentrated feed within the membrane support layer structure. ICP occurs due to the asymmetric nature of TFC membranes wherein the membrane selective layer faces the draw solution in the PRO process. Thicker and denser membrane support layer exacerbates ICP effects thereby hindering water flux during PRO operation. Hence the occurrence of ICP is a huge impediment in osmotic performance of TFC membranes because of which a number of studies have focused on ICP mitigation for osmotic membrane development [10, 11].

A relatively new approach in membrane development is the incorporation of nanomaterials, which can enhance the porosity, permeability, and reactivity of the membranes. These nanomaterials may be either dispersed and immobilized in the membrane support or the selective layer, and form either a mixed matrix membrane (MMM) or a thin film nanocomposite (TFN) membrane, and may serve to modify the morphology and other properties of the membrane [12-14]. Some of the nanomaterials in previous membrane development studies include carbon nanotubes [14-16], silica [17], titanium dioxide [18], titania nanosheets [19], silver [20], graphene oxide [21-23], and metal organic frameworks [24, 25]. Recently, a new

class of Nano-sized materials known as porous organic polymers (POPs) has gained interest for various applications [26]. POPs are porous framework molecules but are only composed of covalently-bonded organic functional groups containing H, C, N, and O, which are considered light elements [27].

Compared to other nanomaterials, POPs exhibit outstanding porosity as well as thermal and chemical stability. Moreover, the hydrophilicity, which is a critical surface property for improving water permeability of a membrane, can be readily improved by either post- or pre-synthetic sulfonate functionalization [28, 29]. All these imply that POPs can be good candidates for the fabrication of high performance TFN membrane featuring high water permeability with an excellent stability. To this end, herein, a specific porous polymer (denoted as PP) reported in our previous work has been synthesized, sulfonated and then incorporated into a TFN membrane to develop a PRO membrane with outstanding osmotic performance [30].

The PP can be facilely prepared from commercially-available monomer *a,a'*-dichloro-*p*-xylene (*p*-DCX) via a one-pot *Friedel-Crafts* alkylation reaction catalyzed by inexpensive $FeCl_3$. PP, which has a high porosity and a robust hydrocarbon structure, can be functionalized by a post-synthetic sulfonation reaction while maintaining the structural integrity. It is noteworthy that, to the best of the authors' knowledge, PP-SO_3H has never been explored as a filler for any TFN membrane. In this study, the PP-SO_3H was incorporated into the selective polyamide layer of an inner-selective TFC hollow fiber PRO membrane. The properties of the PP-SO_3H-incorporated inner-selective TFN hollow fiber PRO membranes and their PRO process performances were evaluated in terms of the nanomaterial loading rates.

EXPERIMENTAL

Materials

1,4-bis(chloromethyl)benzene (*a,a'*-dichloro-*p*-xylene, *p*-DCX, Sigma Aldrich, Singapore), ferric chloride ($FeCl_3$, anhydrous, Sigma Aldrich, Singapore), 1,2-dichloroethane (DCE, Sigma Aldrich, Singapore), chlorosulfonic acid (Tokyo Chemical Industry Co., Ltd., Singapore), methanol (MeOH, VWR Chemicals, Singapore), dichloromethane (DCM, VWR Chemicals, Singapore), and tetrahydrofuran (THF, VWR Chemicals, Singapore) were used for the synthesis of PP-SO_3H.

Polyethersulfone (PES, Veradel® 3000P, M_w = 62000 – 64000 g mol^{-1}, Solvay Specialty Polymers, Republic of Korea) was the polymer for the membrane substrate. N-methyl-2-pyrrolidone (NMP, Merck, Australia) and polyethylene glycol 400 (PEG 400, M_w = 400 g mol^{-1}, Merck, Australia) were the polymer solvent and pore-former, respectively. The as-spun hollow fiber membrane substrates were post-treated with glycerine (99.5 %, Chem-Supply Pty. Ltd., Australia). *m*-phenylenediamine (MPD 99 %, Sigma Aldrich, Australia), trimesic acid trichloride (TMC, 98 %, Sigma Aldrich, Australia), and heptane (99.9 %, anhydrous, Merck, Australia) were utilized for the interfacial polymerization (IP). Different molecular weights of PEG and polyethylene oxide (PEO) (Sigma Aldrich, Australia) were used for pore size distribution measurement. Sodium chloride (NaCl, Chem-Supply Pty. Ltd., Australia) was the chosen inorganic salt for PRO membrane performance evaluation.

Synthesis of PP

Synthesis of PP was first performed according to a method (**Scheme 1**) reported previously [30]. 3.50 g *p*-DCX was mixed in 130 mL DCE to form 20.0 mmol *p*-DCX solution. Anhydrous $FeCl_3$ (3.24 g, 20.0 mmol) was added in the mixture under nitrogen atmosphere. The mixture was placed in vigorous stirring conditions for 1 h at 45°C and 2 h at 80°C. The brown-colored precipitate formed during the reaction was afterwards filtered and thoroughly washed with MeOH and THF alternately until a clear filtrate could be obtained. The PP precipitate was then placed in a vacuum oven at 60°C for 1 d for drying.

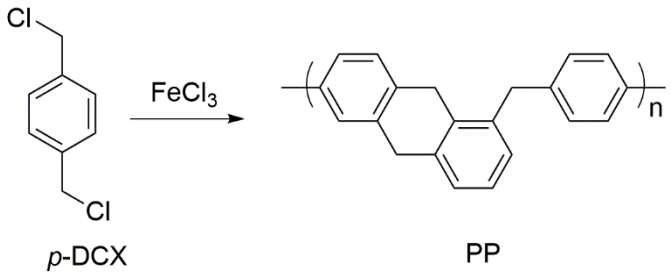

Scheme 1. The self-polymerization of *p*-DCX to synthesize PP.

Sulfonate-functionalization of PP

The PP underwent functionalization modification with chlorosulfonic acid, following a modified method in literature (**Scheme 2**) [31]. 3.0 g of the PP solid was placed with 60 mL DCM in a thoroughly dried flask fitted with a condenser under nitrogen atmosphere. The mixture was stirred until the solution was homogeneous. A mixture containing 20 mL chlorosulfonic acid in 60 mL DCM was added dropwise into the flask at 0°C, after which, the solution was vigorously mixed at ambient temperature for 24 h. The resultant product was collected by

vacuum filtration and rinsed thoroughly with DCM and MeOH. The PP-SO_3H solid was afterwards dried at 80°C for 1 d.

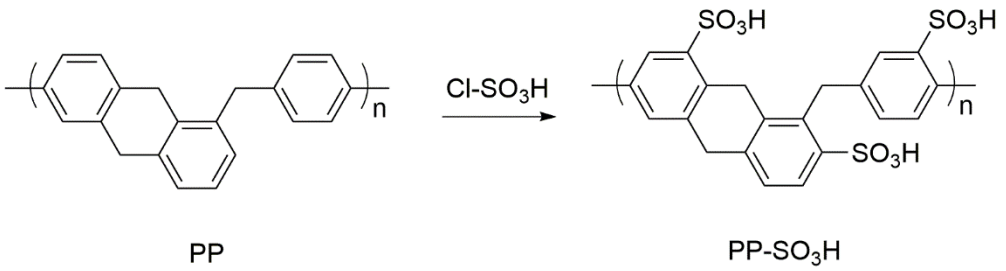

Scheme 2. The functionalization of PP with chlorosulfonic acid to synthesize PP-SO_3H.

PP-SO_3H characterization

Field emission scanning electron microscope (FESEM, Zeiss Supra 55-VP, Germany) and Fourier transform infrared spectrometer (FTIR, IRAffinity-1, Shimadzu, Japan) were used to characterize the synthesized PP-SO_3H nanomaterial. N_2 physisorption studies were performed at 77 K using an Autosorb-6B instrument (Quantachrome, Anton-Paar, Singapore) to determine the surface areas and pore volumes. The amount of sulfonate in PP-SO_3H was quantified using an elemental analyzer (FLASH 2000, Thermo Scientific, Republic of Korea).

PRO hollow fiber membrane substrate preparation

The hollow fiber membrane substrate was prepared by a wet-wet spinning process using a hollow fiber spinning machine (**Figure S1**). The polymer dope solution was prepared with the following composition: 22 wt% PES, 30 wt% PEG 400, 45 wt% NMP, 1.5 wt% LiCl, and 1.5

159 wt% DI water. The bore and polymer dope solutions were supplied separately into their
160 respective channels in the spinning machine. The spinning conditions of the hollow fiber
161 substrate are listed in **Table 1**. The as-spun fibers accumulated on a drum-type rotary winder at a
162 set take-up speed, at an almost free-fall condition. A stepwise approach of the dope solution
163 preparation and hollow fiber membrane substrate preparation can be found in the Supplementary
164 Information. The hollow fibers were afterwards stored in DI water to eliminate solvent residue
165 for approximately 2 d. The spun substrates were then placed in a solution containing 1:1 (w/w)
166 water/glycerol for post-treatment and preservation, followed by air-drying for 2 d, prior to
167 storage and use.

168

169 **Table 1**. The PRO hollow fiber membrane substrate spinning conditions.

Parameter	
Polymer dope solution (wt%)	PES:PEG:NMP:LiCl:DI (22:30:45:1.5:1.5)
Bore solution	DI:NMP (1:1)
Flow rate, dope solution (mL min^{-1})	3.0
Flow rate, bore solution (mL min^{-1})	1.2
Air gap distance (cm)	5.0
Take-up rate (m min^{-1})	1.45 - 1.50
Non-solvent coagulant	Tap water

170

171 ***In situ* interfacial polymerization and PP-SO_3H incorporation**

172 Five hollow fiber membrane substrates, whose effective length is 17 cm, were placed
173 together in a module specifically designed for PRO membrane performance tests. The ends of

the modules were potted with epoxy resin prior to IP and the subsequent membrane performance evaluation.

The polyamide selective layer was synthesized on the lumen (inner surface) of the hollow fiber substrates via IP based on a previous study [32]. Both ends of the modules were tethered to a peristaltic pump (Masterflex HV-77926-10, Cole-Parmer, Australia) to specifically place only the lumen in contact with the precursors of the IP process. An aqueous solution of 2.0 wt% MPD, 0.1 wt% SDS, and various loadings of PP-SO_3H (0 – 0.005 wt%) was first allowed to flow through the membrane lumen for a period of 5 min and a flow rate of 4.5 mL min^{-1}. Excess MPD solution was removed by purging N_2 gas at a pressure of 0.1 bar for 5 min; after which, 0.15 wt% TMC in heptane was then passed through the lumen at a flow rate of 3.0 mL min^{-1} for 5 min to allow complete reaction with the MPD in the pores of the membrane lumen. The TMC unreacted with MPD was afterwards purged out using N_2 gas at a pressure of 0.1 bar for 1 min. The modules were subsequently placed in DI water without any more post-treatment. The membrane modules were stored in cool conditions prior to osmotic tests and characterization. The membrane modules were labelled PP-0, PP-0.001, PP-0.002, and PP-0.005 for PP-SO_3H loading of 0, 0.001, 0.002, and 0.005 wt%, respectively. PP-0 acted as the control TFC membrane, for evaluation of the effect of the incorporation of the nanomaterial.

Membrane characterization

FESEM and FTIR were used to characterize the membrane morphology and chemistry, respectively, following procedure from previous studies [33, 34]. Contact angle measurement using an optical and surface tensiometer (Attension Theta Lite 100, Biolin Scientific, South

196 Korea). This tensiometer has a built-in image processing software to determine membrane
197 surface hydrophilicity. Membrane thickness, membrane tensile strength, porosity, and water
198 uptake ability, were determined according to procedures from a previous study [34]. These
199 properties are tabulated (**Table S1)** in the Supplementary Information.

200

201 **Membrane intrinsic transport parameters determination and osmotic performance**
202 **evaluation**

203 Application of a hydraulic pressure of 10 bar during a reverse osmosis (RO) test was done
204 to determine the following intrinsic transport parameters: pure water permeability coefficient
205 (PWP, A, L m^{-2} h^{-1} bar^{-1}), solute permeability coefficient (B), and structural parameter (S).
206 Osmotic performance was tested with a laboratory-scale PRO system (Cheon Ha Heavy
207 Industries, South Korea) using deionized water (DI water) and 1.0 M NaCl as the feed and draw
208 streams, respectively, at the following pressure range: 0 – 27 bar. Details of the laboratory-scale
209 PRO system are available in a former study [32, 35].

210

211 **RESULTS AND DISCUSSION**

212

213 **PP-SO_3H characterization**

214 A cost-efficient porous organic polymer (PP) obtained by *Friedel-Crafts* alkylation of
215 DCX was then converted into a sulfonated nanomaterial through a post-synthesis
216 functionalization with chlorosulfonic acid to synthesize PP-SO_3H. **Figure 1** shows the

morphology of the synthesized PP-SO_3H. The spherically shaped PP-SO_3H each has a size of approximately 90-100 nm; thus, it is suitable for incorporation within the polyamide selective layer, which typically has a thickness of 150 nm.

The FTIR spectra of PP and PP-SO_3H are shown in **Figure 2**. A –CH stretching at 2920 cm^{-1} and a sharp peak between 1600 and 1500 cm^{-1} were observed, corresponding to the saturated –CH2– and –C=C– groups, respectively. The stretching vibrations appearing between 1050 and 1040 cm^{-1}, which are only present for the spectrum of PP-SO3H, are assigned to O=S=O indicating the successful introduction of sulfonate groups. The surface area and pore volume values calculated from the N_2 physisorption studies at 77 K are tabulated in **Table 2**. The pore volume and surface area values signify the microporous and mesoporous characteristic of PP-SO_3H. After elemental analysis, the amount of sulfonate in the porous polymer nanomaterial after sulfonate functionalization was found to be 2.80 mmol g^{-1}.

229 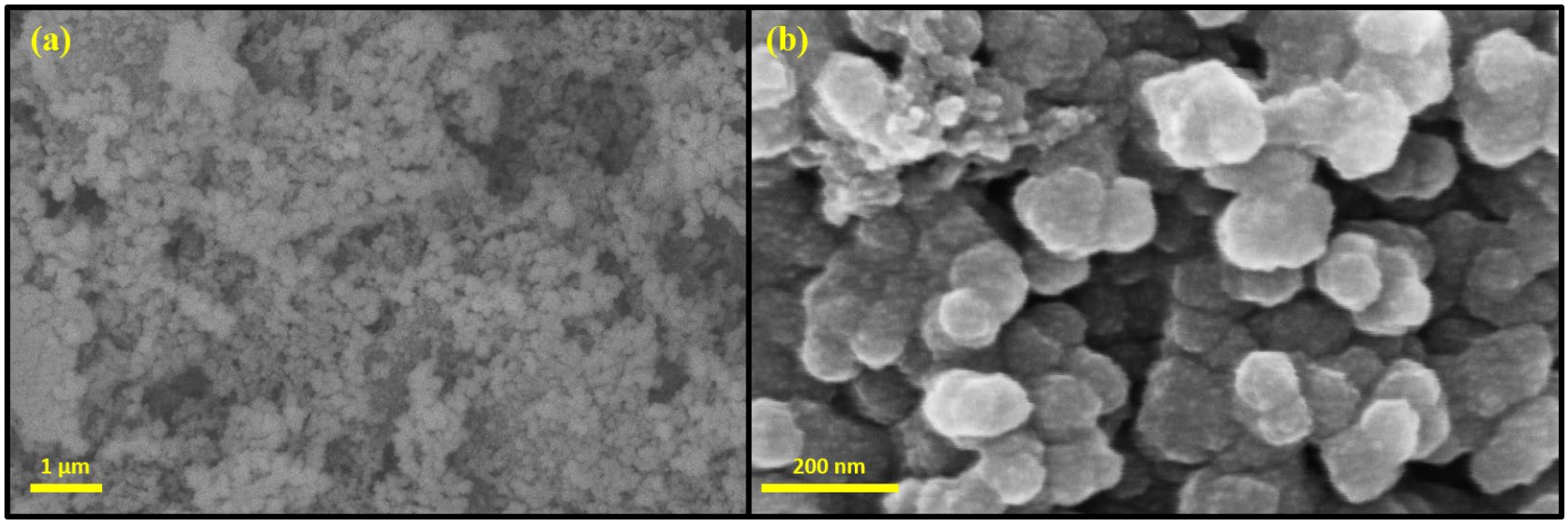

230 **Figure 1.** FESEM images of PP-SO_3H at two different magnifications.

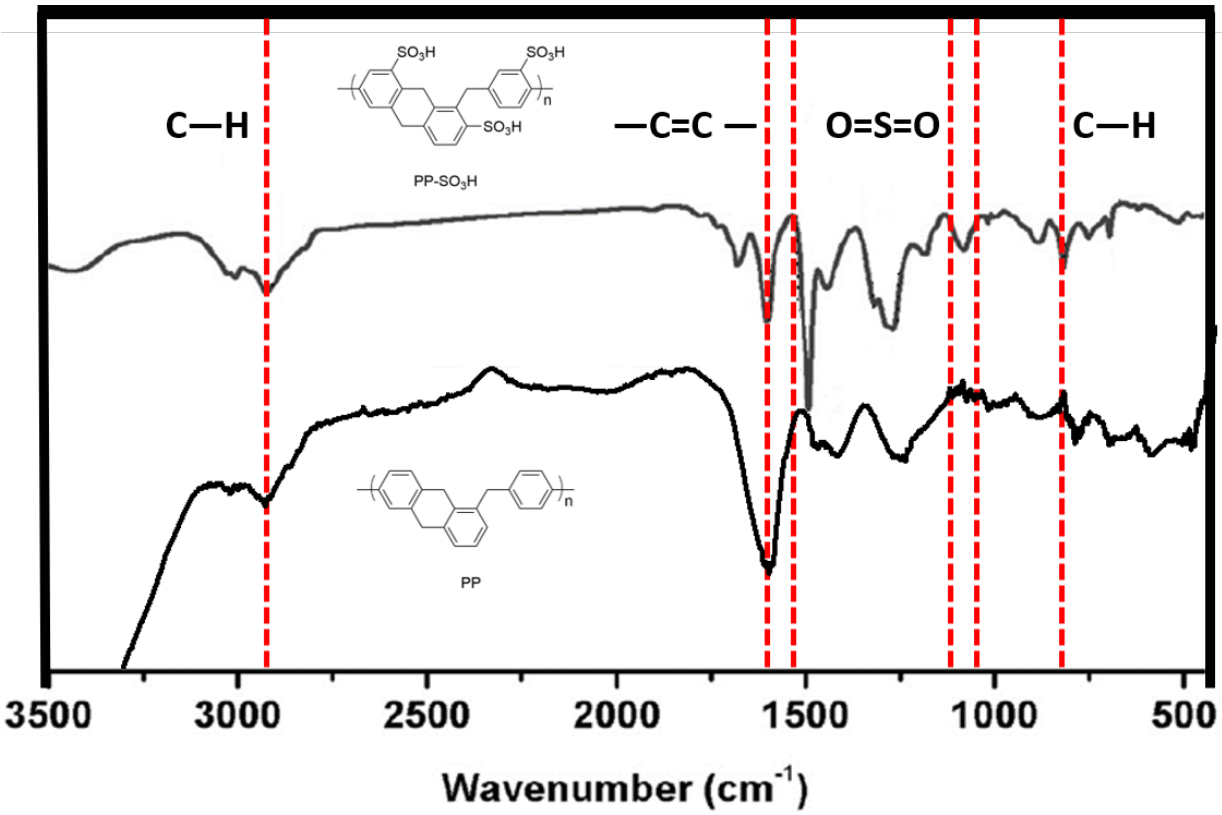

Figure 2. The FTIR spectra of the synthesized PP and PP-SO_3H, formed after the sulfonate functionalization of PP. The chemical structure of PP and PP-SO_3H are also shown inset.

Table 2. The surface area and pore volume values of PP and PP-SO_3H.

Samples	S_{BET}[†]	S_{micro}[‡]	V_{micro}[‡]	V_{total}[§]
PP	1480 m^2 g^{-1}	866 m^2 g^{-1}	0.402 cm^3 g^{-1}	2.60 cm^3 g^{-1}
PP-SO_3H	1090 m^2 g^{-1}	680 m^2 g^{-1}	0.313 cm^3 g^{-1}	1.48 cm^3 g^{-1}

[†]The surface area determined over the relative pressure (P/P^0) range of 0.05-0.2 using Brunauer-Emmett-Teller method.

239 ‡The microporous surface area and pore volume determined over P/P^0 range of 0.4-0.6 using *t*-
240 plot method analysis for micropores.

241 §The total pore volume determined at P/P^0 of 0.99.

242

243 **Membrane characterization**

244 The surface of the membranes was characterized using FTIR spectroscopy to determine the
245 effect of incorporation of PP-SO_3H on the surface chemistry. As shown in **Figure 3**, FTIR
246 spectrum suggests the presence of the polyamide selective layer on all the TFC (PP-0) and TFN
247 (PP-0.001, PP-0.002, and PP-0.005) membranes. The carbonyl C–N group of the polyamide was
248 evident for all the membrane samples, due to the presence of stretching at 1615 cm^{-1}, as well as
249 the vibrations around 1440 cm^{-1}. Vibrations between 1600 and 1450 cm^{-1} indicate the
250 unsaturated –C=C– and $–CH_2$ groups. The TFN membranes were observed to exhibit the O=S=O
251 stretching vibrations between 1050 and 1040 cm^{-1}, indicating the presence of the sulfonate-
252 functionalized PP-SO_3H. FTIR spectroscopy was able to show the successful incorporation of
253 PP-SO_3H in the TFN PRO membranes.

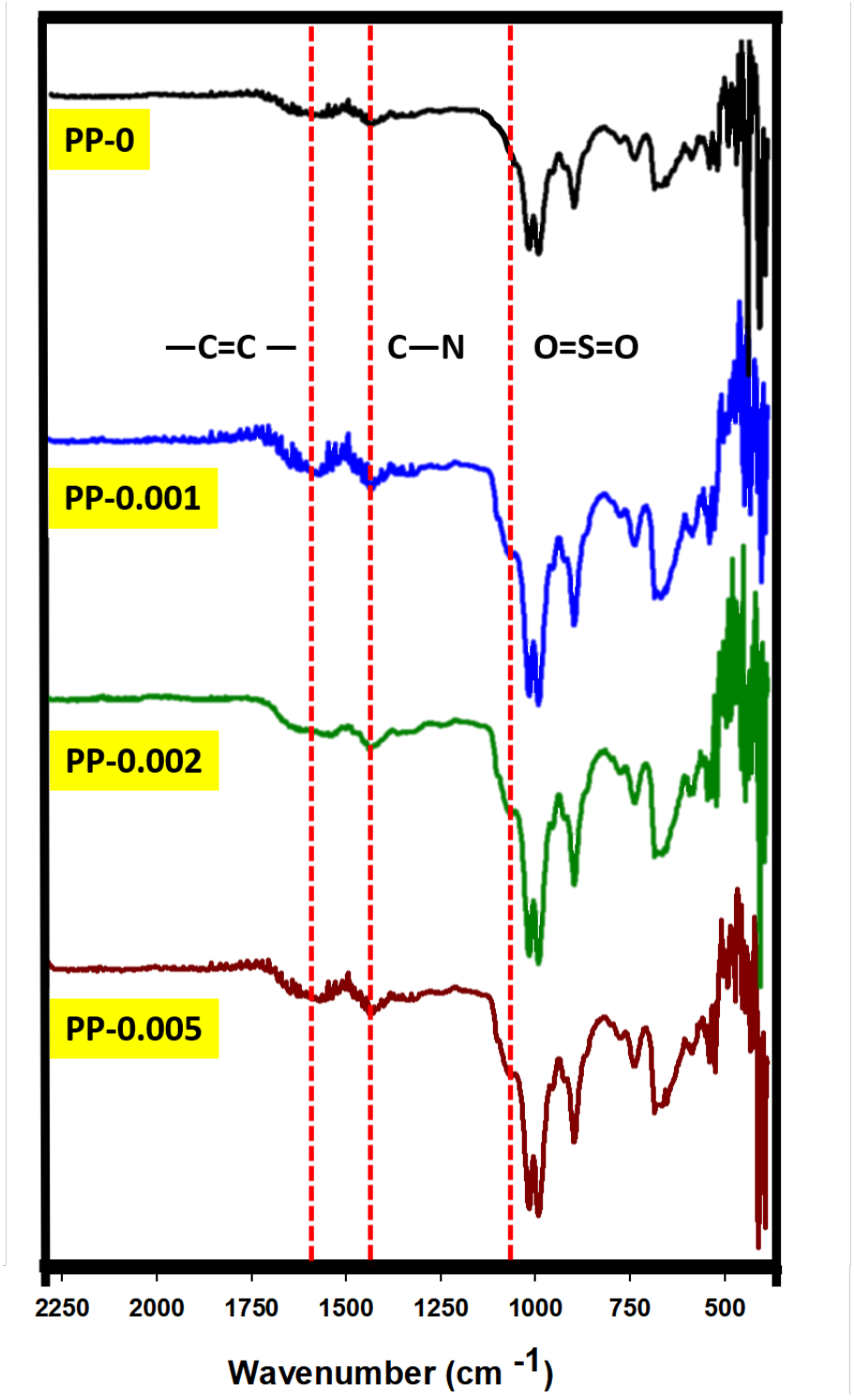

254

255 **Figure 3.** The FTIR spectra of the TFC (PP-0) and TFN (PP-0.001, PP-0.002, and PP-0.005)

256 PRO membranes.

The morphologies of the lumen (inner surface), shell (outer surface), and cross-section of the hollow fiber membrane substrates were characterized using FESEM, and are shown in **Figure 4**. Using the FESEM images, the average thickness, total diameter, and inner diameter of the spun hollow fiber substrates were determined to be 324 ± 12, 1309 ± 148, and 647 ± 29 μm, respectively (shown in **Table S1** in the Supplementary Information, along with the hollow fiber substrate's other properties). The cross-sectional FESEM images show that the hollow fiber is highly porous, with an asymmetrical structure consisting of finger-like pore structures, which are typical of most porous membrane supports for osmotic membranes. The shell and lumen sides of the hollow fiber, on the other hand, show highly different morphologies with each other. The shell side of the hollow fiber membrane substrates was designed to be highly porous for faster transport of water during the osmotic process, thereby reducing ICP effects. The outer surface on the shell side appears rough and highly porous, while the lumen (inner) side, on the contrary, is found to be much denser with the presence of skin layer and much smaller surface pores. This is a result of the instantaneous phase inversion occurring during the simultaneous extrusion of the polymer dope and bore solutions during the hollow fiber spinning process. The use of the bore solution mixture of DI water and NMP, which is a weaker non-solvent than just pure DI water, caused phase inversion to occur at a slower rate, resulting in the existence of smaller macrovoid structures and more sponge-like surface pores close to the lumen side [36].

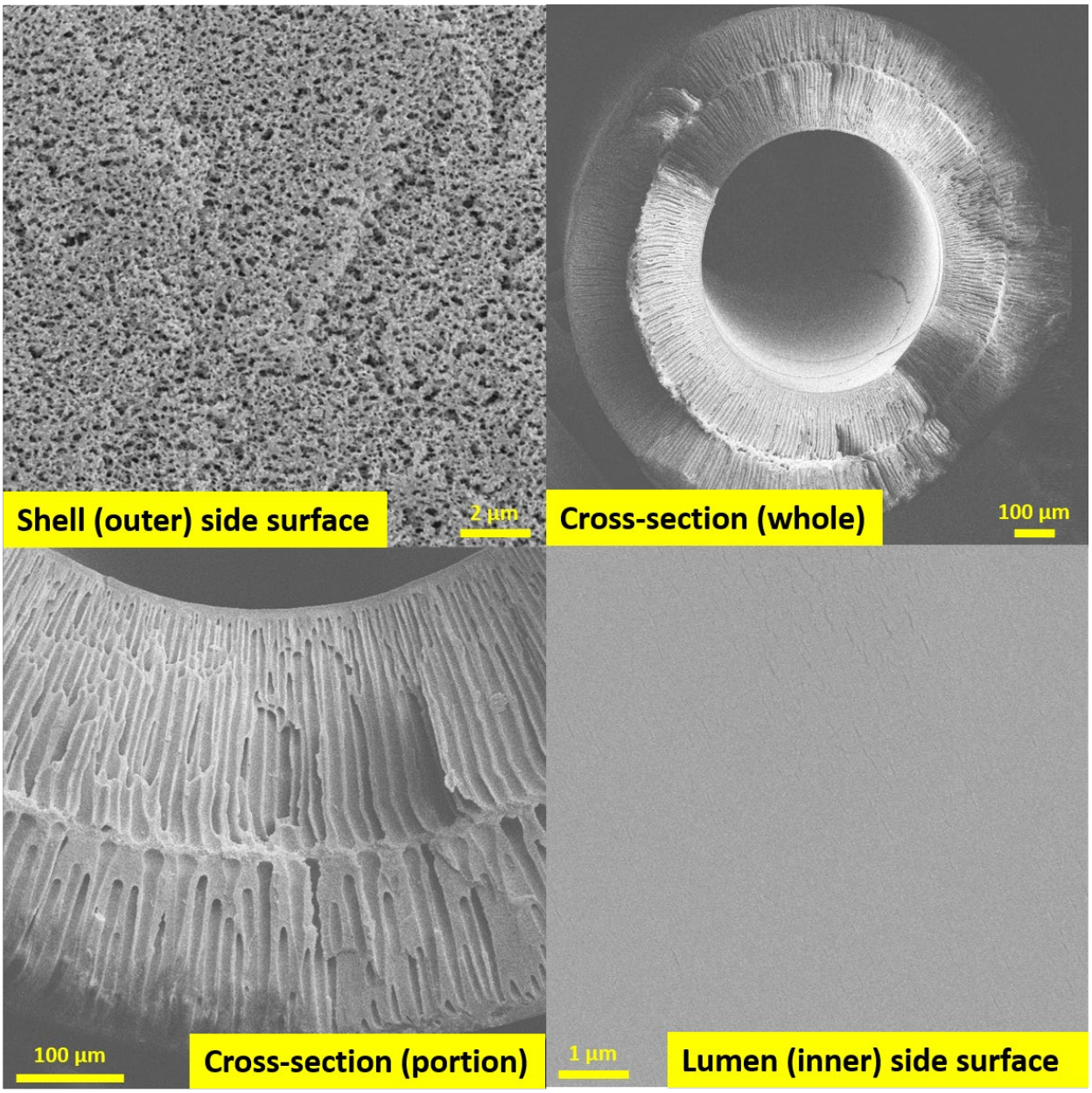

277

278 **Figure 4.** The shell (outer) side surface, cross section, and lumen (inner) side surface

279 morphologies of the as-spun hollow fiber membrane substrates characterized using FESEM

280 imaging.

281

Figure 5 shows the polyamide selective layer surface of the TFC (PP-0) and TFN (PP-0.001, PP-0.002, and PP-0.005) membranes. All the membranes exhibited the presence of the selective layer, as shown by the ridge-and-valley structures which are characteristics of a polyamide, thus confirming that interfacial polymerization has occurred between MPD and TMC solutions. The PP-SO_3H nanoparticles are incorporated into the polyamide through the aqueous MPD solution thus appear to be fully embedded well within the polyamide layer.

The presence of hydrophilic nanomaterials, such as sulfonate-functionalized PP-SO_3H, in the polyamide effectively enhances the surface hydrophilicity and therefore affinity of the members to water [35]. To determine if this was the case in this study, the static water contact angle was measured on the membrane surfaces. Lower contact angles generally corresponds to higher degree of hydrophilicity; however, the contact angle is not only due to hydrophilicity effect but also its surface roughness, such that smoother surfaces are observed to have lower contact angles [33]. The contact angle measurements can be found also in **Figure 5** (inset). The TFC membrane exhibited a contact angle measurement of 64°, which decreased, albeit to a small degree, with the increase in PP-SO_3H loading. Sample PP-0.005, which has a PP-SO_3H loading of 0.005 wt %, showed the lowest contact angle of about 40°. This observed increase in hydrophilicity of the PP-0.005 TFN PRO membrane is a direct result of the presence of the hydrophilic functionalized nanoparticles. It is also noteworthy that the marked decrease in contact angle measurements is not linear or directly proportional to the PP-SO_3H loading rate, because aside from the random deposition of the POP nanomaterial on the polyamide layer, the incorporation of nanomaterials likewise increases the surface roughness of the membrane [37].

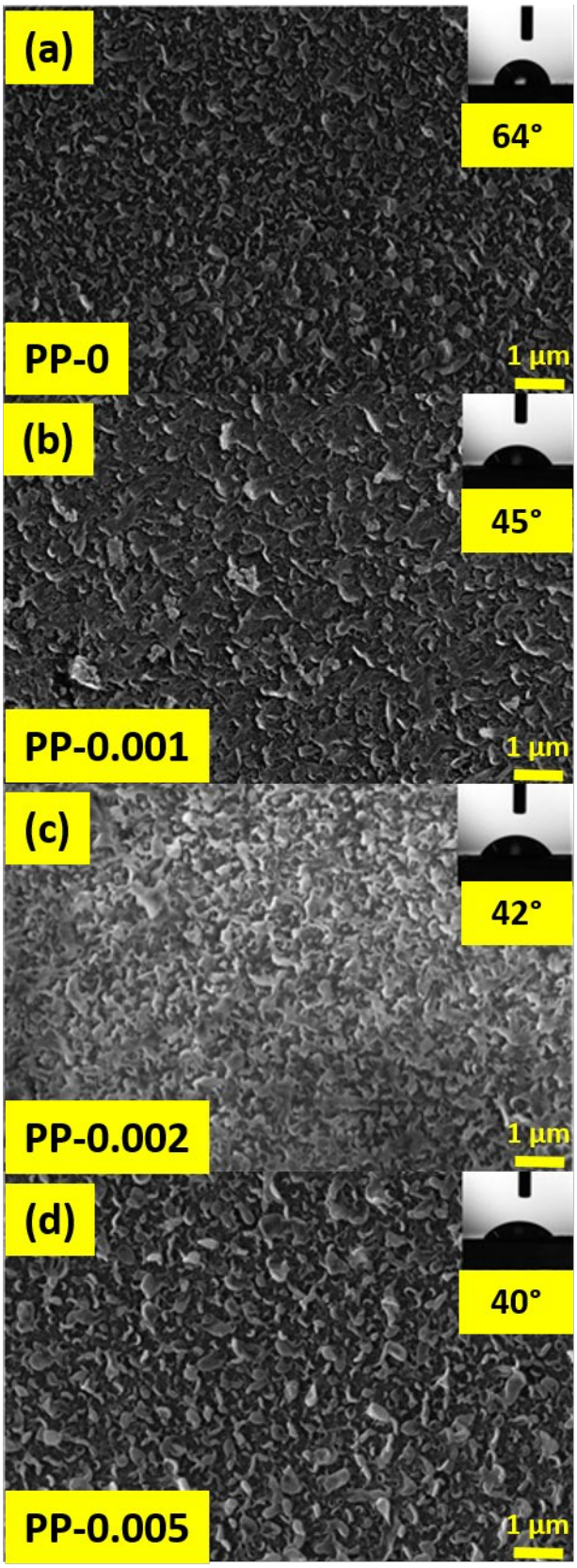

304

Figure 5. The selective layer morphologies for (a) PP-0, (b) PP-0.001, (c) PP-0.002, and (d) PP-0.005 PRO hollow fiber TFC and TFN membranes characterized using FESEM imaging. Surface contact angle values of each membrane were included inset.

Membrane intrinsic transport parameters

The intrinsic membrane transport parameters of the TFC and TFN PRO membranes are presented in **Table 3**. While all the A values lie within the range of 1.37 – 1.85 L m^{-2} h^{-1} bar^{-1}, there was a noticeable increase for the PP-SO_3H-incorporated TFN membranes compared to pristine TFC membrane. This is most likely due to enhanced hydrophilicity of the TFN membrane surface as a result of the incorporation of a hydrophilic and porous PP-SO_3H nanomaterial. Also, previous studies noted that there are also interstices between the nanomaterial and the polyamide, providing additional channels for water transport [35, 38]. The highest A value of 1.85 L m^{-2} h^{-1} bar^{-1} was observed for PP-0.002. It was hypothesized that water permeability could increase with nanomaterial loading, due to the effective increase in hydrophilicity and availability of higher number of pores and interstices from the nanomaterial itself. However, this was not observed in this study and hence it can be said that there is an optimal loading rate for nanomaterial incorporation within the polyamide layer that can provide the best membrane permeability.

The B values, on the other hand, showed an upward trend as the PP-SO_3H loading increased. PP-0 exhibited a B value of 0.35 L m^{-2} h^{-1} which increased to 1.57 L m^{-2} h^{-1} for PP-0.005. Higher water permeability is generally associated with correspondingly higher salt permeability and besides higher porosity of the PP-SO_3H nanoparticles also likely enhanced the

transport of solute particles. Consequently, the solute rejection decreased from 96% for PP-0 to 88% for PP-0.005.

Lastly, the *S* value was also evaluated for all the membrane samples, and it was found that the *S* value of 743 μm for PP-0 membrane slightly decreased with the increase in nanomaterial loading. This can be attributed to the modification of surface chemical composition, which showed significantly higher hydrophilic character.

Table 3. The intrinsic membrane transport parameters of the TFC (PP-0) and the PP-SO_3H. incorporated TFN (PP-0.001, P-0.002, and P-0.005) membranes.

Membrane	$A^{\dagger}$ (L m^{-2} h^{-1} bar^{-1})	$B^{\ddagger}$ (L m^{-2} h^{-1})	*B/A* (bar)	$R^{\ddagger}$ (%)	*S* (μm)
PP-0	1.37 ± 0.19	0.35	0.26	96.1 ± 1.1	743
PP-0.001	1.51 ± 0.13	0.65	0.43	93.5 ± 0.9	689
PP-0.002	1.85 ± 0.12	1.41	0.76	90.3 ± 1.3	652
PP-0.005	1.76 ± 0.24	1.57	0.89	88.2 ± 1.3	624

†Pure water permeability coefficient, *A*, was determined at ΔP = 10 bar with DI water as feed.

‡Solute permeability coefficient, *B*, and solute rejection, R, were determined at ΔP = 10 bar with 2000 mg L^{-1} NaCl as the feed.

Performance of membranes for PRO process

The TFC and the TFN hollow fiber PRO membranes were pre-stabilized prior to osmotic performance evaluation. The pre-stabilization step was performed at a hydraulic pressure slightly below the burst pressure to avoid instant breakage of the polyamide selective layer membranes

during PRO operation [32, 39]. The hollow fiber membranes in this study were found to burst between 17 and 18 bar, thus the PRO membranes were pre-stabilized at 15 bar under RO mode (selective layer facing the pressurized stream) for 60 min using DI water as feed. The pre-stabilization stage allows the simultaneous expansion and compaction of both the hollow fiber membrane substrate and the polyamide layer. These have resulted in elastic stretching of the polymeric substrate and the thinning of both substrate and selective layer, hereby increasing the total effective membrane area [32]. The effective thinning of the membrane then effectively reduces water transport resistance, thus increasing water permeability, as well.

Figure 6 shows the osmotic behavior of the inner-selective PRO membranes in terms of water flux (J_w, expressed as L m^{-2} h^{-1}), specific reverse salt flux (J_s/J_w, expressed as g L^{-1}), and power density (W, expressed as W m^{-2}). DI water and 1.0 M NaCl were used as the feed and draw streams, respectively, during the PRO operation with the polyamide selective layer facing the direction of the pressurized draw stream.

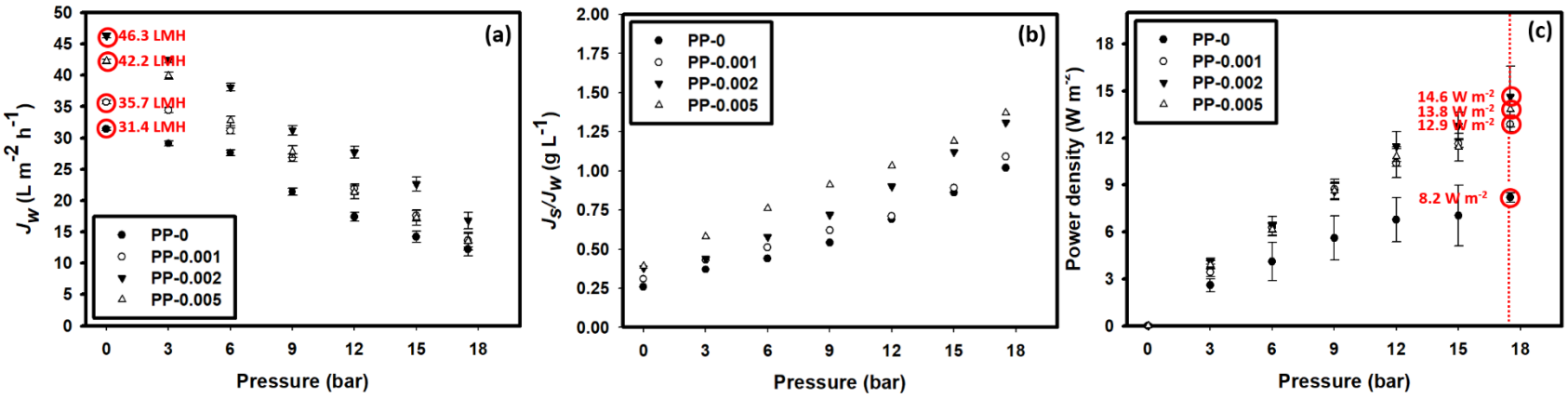

357

358 **Figure 6.** The osmotic performance during PRO operation at varying applied hydraulic pressure values, expressed in (a) water flux

359 (J_w), (b) specific reverse salt flux (J_s/J_w), and (c) power density, for PP-0, PP-0.001, PP-0.002, and PP-0.005. DI water and 1.0 M

360 NaCl were the feed and draw, respectively, during PRO operation.

Figures 6.a and 6.b show the membranes' water flux and specific reverse salt flux performance at varying applied hydraulic pressures. The J_w values at $\Delta P = 0$ were consistent with the A values, that there was a marked increase upon incorporation of PP-SO_3H until a 0.002 wt % loading and declined at 0.005 wt% loading. The hydrophilic water-selective channels of PP-SO_3H enhanced the membrane wetting capability of the membrane, and water transport, as well. The –SO_3H functional group of the POP nanomaterial is able to create strong H-bonds with the O–H bonds of water molecules. One drawback of TFC membranes is that the dense polyamide thin film layer usually hinders mass transport due to its lack of solvent transport channels as the PA layer is generally considered non-porous membrane. The incorporation of nanomaterials, such as PP-SO_3H, not only embeds highly porous nanomaterials, but also disrupts the dense structure of the polyamide, making interstices between the nanomaterial and the polyamide, maximizing the fractional free volume for water transport [40]. The highest water flux of 46.3 L m^{-2} h^{-1} was observed for PP-0.002, a dramatic improvement compared to PP-00 with 31.4 L m^{-2} h^{-1}. Incorporation of 0.001 wt% of the PP-SO_3H elevated the J_w to 35.71 L m^{-2} h^{-1}. The J_w decreases slightly for nanomaterial loading above 0.002 wt% and this is conceivably attributed to the agglomeration of the nano-sized particles, ergo reducing permeability as evident from the 42.2 L m^{-2} h^{-1} water flux value of PP-0.005.

As the hydraulic pressure applied during the PRO operation increases, J_w gradually decreases for all membrane samples which is expected due to reduction in the driving force. This continues until the applied hydraulic pressure is identical to the osmotic pressure difference between the draw and feed streams. As pressure is continuously applied on the membrane, the membrane sustained damage from membrane compaction and stretching, as well as the thinning of the polyamide layer. During the pre-stabilization step, the membrane was subjected to a

384 pressure less than the burst pressure for it to be compacted and stretched, without breaking;
385 however, due to the elasticity of the polymeric membrane substrate, the membrane bounces back
386 to its original shape and properties. During the continuous PRO operation wherein, hydraulic
387 pressure is constantly applied onto the polyamide selective layer of the membrane, the membrane
388 starts to incur irreversible defects and damage, until it can no longer sustain the damage and
389 eventually bursts. The ability of a membrane to sustain damage despite higher applied hydraulic
390 pressure is a measurement of its robustness, thus the burst pressure is used to evaluate the
391 membrane robustness in previous PRO membrane development studies [35, 41]. Membrane
392 robustness is an important parameter that needs to be considered for the long-term PRO
393 operation under pressurized environment.

394 Due to the enhanced water permeability of the membranes, one expected trade-off in the
395 form of lower solute rejection due to enhanced solute permeability. Although a trade-off between
396 permeability and selectivity was observed for PP-SO_3H incorporated TFN membranes however,
397 the J_s/J_w values of 0.2 g L^{-1} for PP-0, 0.3 g L^{-1} for PP-0.001, and 0.4 g L^{-1} for PP-0.002 are
398 encouragingly within the ranges reported in the literature. This increasing J_s/J_w trend is in fact
399 consistent with the B values earlier discussed earlier. In the osmotic process, a much higher
400 amount of water is expected to move from the feed to the draw solution as compared to the
401 quantity of salt diffusing from the draw to the feed and this perhaps explains the reason for not so
402 significant increase in the J_s/J_w values. This is especially true since water molecules are much
403 smaller than NaCl molecules, so water molecules could penetrate the pores and interfaces of the
404 nanomaterial and the membrane [42]. Furthermore, the hydrophilic character of the nanomaterial
405 incorporated in the polyamide helps to enhance attraction of water molecules. POP
406 nanomaterials, such as PP-SO_3H are known to be molecular sieves that the molecule has the

ability to sieve out other molecules of larger size. This way, despite the supposed drawback of selectivity, we were able to observe that the TFN membranes were able to limit the occurrence of reverse salt permeability and maintain satisfactory salt rejection ability.

As applied hydraulic pressure on the draw stream increases, it was also observed consistently for all membrane samples that selectivity declines as indicated by the steady increase in the J_s/J_w values. The reverse draw salt transport is a function of concentration difference between the draw solution and feed solution which does not change much however the water flux from the feed is retarded due to the presence of applied pressure on the draw stream and hence the J_s/J_w values increases proportionately with the applied pressure. Besides, damage of the polyamide selective layer of the membrane is also highly likely due to compaction, stretching, and thinning out due to the applied pressure thereby allowing more transport channels for solute particles to pass through.

Figure 6.c shows the power density or W values of the TFC and TFN membranes at different applied hydraulic pressures. The power density is a straightforward evaluation of the osmotic power generation capacity of the membranes. It is directly related to the water permeability and the applied hydraulic pressure, as well, until a certain point. As the applied hydraulic pressure increases, the power density was found to increase at a hyperbolic trend, until the maximum W value is reached, typically at applied hydraulic pressure equals to half the osmotic pressure difference between the draw and feed solutions. Since the PRO hollow fiber membranes in this study were unable to withstand hydraulic pressure beyond 18 bar, hence these membranes could not be tested at the applied hydraulic pressure to achieve maximum W value. The highest W value obtained for the TFC PRO membrane in this study was 8.2 W m^{-2} at ΔP =

17 bar. Incorporation of 0.002 wt% of PP-SO_3H resulted in a significant increase of the highest W value of 14.6 W m^{-2} at the same applied hydraulic pressure.

This membrane performance evaluation results suggest that incorporation of highly porous and hydrophilic nano-sized particles in the polyamide selective layer can effectively enhance water permeability and osmotic power generation of the hollow fiber PRO membranes.

CONCLUSION

In this study, a hydrophobic porous polymer nanomaterial, PP was functionalized using chlorosulfonic acid to form sulfonate-functionalized PP-SO_3H with hydrophilic properties. PP-SO_3H was incorporated in the polyamide layer on PES hollow fiber membrane substrate to develop a high-performance TFN PRO membranes. The following conclusions are drawn from this study:

1. The incorporation of functionalized nanomaterials, such as PP-SO_3H, in the polyamide layer effectively modifies the surface chemistry of the selective layer of the osmotic membrane;
2. The presence of highly porous and hydrophilic nanomaterials, such as PP-SO_3H, into the polyamide selective layer significantly enhances water affinity and water permeability of the TFN PRO membranes as a result of enhanced water transport mechanism across the membranes;
3. Despite the enhanced water permeability across the membranes, the salt rejection of the polyamide layer remained satisfactory;

The results suggest that the incorporation of a highly porous and hydrophilic functionalized nanomaterial into the polyamide selective layer is a promising method to develop highly effective TFN membranes for sustainable osmotic power generation. This study has shown that the engineering of the polyamide selective layer by incorporation of a functionalized nano-sized material, such as PP-SO_3H, could effectively result in the functionalization of the TFN membrane surface, as well as enhancement of separation properties. Given the small amounts required of the nanomaterial to be incorporated in the polyamide layer and the enhancement of performance despite the low loading rates, it can be said that functionalized nanomaterial incorporation could be another step toward the development of high-performance membranes and larger-scale application of PRO.

ACKNOWLEDGEMENT

This research was supported by a grant from the Qatar National Research Fund under its National Priorities Research Program award number NPRP 10-1231-160069 and the Australian Research Council (ARC) Industrial Transformation Research Hub (IH170100009).

REFERENCES

[1] A.P. Straub, A. Deshmukh, M. Elimelech, Pressure-retarded osmosis for power generation from salinity gradients: Is it viable?, Energy Environ. Sci., (2015).
[2] F. Volpin, R.R. Gonzales, S. Lim, N. Pathak, S. Phuntsho, H.K. Shon, GreenPRO: A novel fertiliser-driven osmotic power generation process for fertigation, Desalination, 447 (2018) 158-166.
[3] R.R. Gonzales, J.S. Kim, S.-H. Kim, Optimization of dilute acid and enzymatic hydrolysis for dark fermentative hydrogen production from the empty fruit bunch of oil palm, International Journal of Hydrogen Energy, 44 (2019) 2191-2202.
[4] D.I. Kim, R.R. Gonzales, P. Dorji, G. Gwak, S. Phuntsho, S. Hong, H. Shon, Efficient recovery of nitrate from municipal wastewater via MCDI using anion-exchange polymer coated electrode embedded with nitrate selective resin, Desalination, 484 (2020) 114425.

[5] C. Klaysom, T.Y. Cath, T. Depuydt, I.F.J. Vankelecom, Forward and pressure retarded osmosis: potential solutions for global challenges in energy and water supply, Chemical Society Reviews, 42 (2013) 6959-6989.
[6] S. Zhang, P. Sukitpaneenit, T.-S. Chung, Design of robust hollow fiber membranes with high power density for osmotic energy production, Chemical Engineering Journal, 241 (2014) 457-465.
[7] N.Y. Yip, A. Tiraferri, W.A. Phillip, J.D. Schiffman, L.A. Hoover, Y.C. Kim, M. Elimelech, Thin-film composite pressure retarded osmosis membranes for sustainable power generation from salinity gradients, Environmental Science & Technology, 45 (2011) 4360-4369.
[8] S. Chou, R. Wang, L. Shi, Q. She, C. Tang, A.G. Fane, Thin-film composite hollow fiber membranes for pressure retarded osmosis (PRO) process with high power density, Journal of Membrane Science, 389 (2012) 25-33.
[9] G. Han, S. Zhang, X. Li, T.-S. Chung, Progress in pressure retarded osmosis (PRO) membranes for osmotic power generation, Progress in Polymer Science, 51 (2015) 1-27.
[10] L. Huang, J.T. Arena, M.T. Meyering, T.J. Hamlin, J.R. McCutcheon, Tailored multi-zoned nylon 6,6 supported thin film composite membranes for pressure retarded osmosis, Desalination, 399 (2016) 96-104.
[11] X. Song, Z. Liu, D.D. Sun, Energy recovery from concentrated seawater brine by thin-film nanofiber composite pressure retarded osmosis membranes with high power density, Energy & Environmental Science, 6 (2013) 1199-1210.
[12] H.-g. Choi, M. Son, H. Choi, Integrating seawater desalination and wastewater reclamation forward osmosis process using thin-film composite mixed matrix membrane with functionalized carbon nanotube blended polyethersulfone support layer, Chemosphere, 185 (2017) 1181-1188.
[13] L. Wang, X. Song, T. Wang, S. Wang, Z. Wang, C. Gao, Fabrication and characterization of polyethersulfone/carbon nanotubes (PES/CNTs) based mixed matrix membranes (MMMs) for nanofiltration application, Applied Surface Science, 330 (2015) 118-125.
[14] M. Amini, M. Jahanshani, A. Rahimpour, Synthesis of novel thin film nanocomposite (TFN) forward osmosis membranes using functionalized multi-walled carbon nanotubes, Journal of Membrane Science, 435 (2013) 233-241.
[15] X. Song, L. Wang, C.Y. Tang, Z. Wang, C. Gao, Fabrication of carbon nanotubes incorporated double-skinned thin film nanocomposite membranes for enhanced separation performance and antifouling capability in forward osmosis process, Desalination, 369 (2015) 1-9.
[16] L. Deng, Q. Wang, X. An, Z. Li, Y. Hu, Towards enhanced antifouling and flux performances of thin-film composite forward osmosis membrane via constructing a sandwich-like carbon nanotubes-coated support, Desalination, 479 (2020) 114311.
[17] M. Tian, Y.-N. Wang, R. Wang, A.G. Fane, Synthesis and characterization of thin film nanocomposite forward osmosis membranes supported by silica nanoparticle incorporated nanofibrous substrate, Desalination, 401 (2017) 142-150.
[18] M. Ghanbari, D. Emadzadeh, W.J. Lau, T. Matsuura, M. Davoody, A.F. Ismail, Super hydrophilic TiO2/HNT nanocomposites as a new approach for fabrication of high performance thin film nanocomposite membranes for FO application, Desalination, 371 (2015) 104-114.
[19] N.A. Ahmad, P.S. Goh, K.C. Wong, A.K. Zulhairun, A.F. Ismail, Enhancing desalination performance of thin film composite membrane through layer by layer assembly of oppositely charged titania nanosheet, Desalination, 476 (2020) 114167.
[20] X. Liu, S. Qi, Y. Li, L. Yang, B. Cao, C.Y. Tang, Synthesis and characterization of novel antibacterial silver nanocomposite nanofiltration and forward osmosis membranes based on layer-by-layer assembly, Water Research, 47 (2013) 3081-3092.

[21] A. Soroush, W. Ma, M. Cyr, M.S. Rahaman, B. Asadishad, N. Tufenkji, In situ silver decoration on graphene oxide-treated thin film composite forward osmosis membranes: Biocidal properties and regeneration potential, Environmental Science & Technology Letters, 3 (2016) 13-18.
[22] H.M. Hegab, A. ElMekawy, T.G. Barclay, A. Michelmore, L. Zou, C.P. Saint, M. Ginic-Markovic, Fine-tuning the surface of forward osmosis membranes via grafting graphene oxide: Performance patterns and biofouling propensity, ACS Applied Materials & Interfaces, 7 (2015) 18004-18016.
[23] Y. Kang, M. Obaid, J. Jang, I.S. Kim, Sulfonated graphene oxide incorporated thin film nanocomposite nanofiltration membrane to enhance permeation and antifouling properties, Desalination, 470 (2019) 114125.
[24] M. Kadhom, W. Hu, B. Deng, Thin film nanocomposite membranes filled with metal-organic frameworks UiO-66 and MIL-125 nanoparticles for water desalination, Membranes, 7 (2017) 31.
[25] D. Ma, S.B. Peh, G. Han, S.B. Chen, Thin-film nanocomposite membranes incorporated with super-hydrophilic metal-organic framework (MOF) UiO-66: Toward enhancement of water flux and salt rejection, ACS Applied Materials & Interfaces, 9 (2017) 7523-7534.
[26] S. Kitagawa, R. Kitaura, S.-i. Noro, Functional porous coordination polymers, Angewandte Chemie International Edition, 43 (2004) 2334-2375.
[27] L. Zou, Y. Sun, S. Che, X. Yang, X. Wang, M. Bosch, Q. Wang, H. Li, M. Smith, S. Yuan, Z. Perry, H.C. Zhou, Porous organic polymers for post-combustion carbon capture, Adv. Mater., 29 (2017) 1700229.
[28] W. Lu, D. Yuan, J. Sculley, D. Zhao, R. Krishna, H.C. Zhou, Sulfonate-grafted porous polymer networks for preferential CO2 adsorption at low pressure, J Am Chem Soc, 133 (2011) 18126-18129.
[29] S. Chandra, T. Kundu, K. Dey, M. Addicoat, T. Heine, R. Banerjee, Interplaying Intrinsic and Extrinsic Proton Conductivities in Covalent Organic Frameworks, Chem. Mat., 28 (2016) 1489-1494.
[30] Y. Yang, C.Y. Chuah, L. Nie, T.-H. Bae, Enhancing the mechanical strength and CO_2/CH_4 separation performance of polymeric membranes by incorporating amine-appended porous polymers, J. Membr. Sci., 569 (2019) 149-156.
[31] J. Li, X. Wang, G. Chen, D. Li, Y. Zhou, X. Yang, J. Wang, Hypercrosslinked organic polymer based carbonaceous catalytic materials: Sulfonic acid functionality and nano-confinement effect, Applied Catalysis B: Environmental, 176-177 (2015) 718-730.
[32] M.J. Park, S. Lim, R.R. Gonzales, S. Phuntsho, D.S. Han, A. Abdel-Wahab, S. Adham, H.K. Shon, Thin-film composite hollow fiber membranes incorporated with graphene oxide in polyethersulfone support layers for enhanced osmotic power density, Desalination, 464 (2019) 63-75.
[33] M.J. Park, R.R. Gonzales, A. Abdel-Wahab, S. Phuntsho, H.K. Shon, Hydrophilic polyvinyl alcohol coating on hydrophobic electrospun nanofiber membrane for high performance thin film composite forward osmosis membrane, Desalination, 426 (2018) 50-59.
[34] R.R. Gonzales, M.J. Park, L. Tijing, D.S. Han, S. Phuntsho, H.K. Shon, Modification of nanofiber support layer for thin film composite forward osmosis membranes via layer-by-layer polyelectrolyte deposition, Membranes, 8 (2018) 70-84.
[35] R.R. Gonzales, M.J. Park, T.-H. Bae, Y. Yang, A. Abdel-Wahab, S. Phuntsho, H.K. Shon, Melamine-based covalent organic framework-incorporated thin film nanocomposite membrane for enhanced osmotic power generation, Desalination, 459 (2019) 10-19.

[36] G. Han, P. Wang, T.-S. Chung, Highly robust thin-film composite pressure retarded osmosis (PRO) hollow fiber membranes with high power densities for renewable salinity-gradient energy generation, Environmental Science & Technology, 47 (2013) 8070-8077.
[37] T.-Y. Liu, H.-G. Yuan, Y.-Y. Liu, D. Ren, Y.-C. Su, X. Wang, Metal-organic framework nanocomposite thin films with interfacial bindings and self-standing robustness for high water flux and enhanced ion selectivity, ACS Nano, 12 (2018) 9253-9265.
[38] C. Wang, Z. Li, J. Chen, Z. Li, Y. Yin, L. Cao, Y. Zhong, H. Wu, Covalent organic framework modified polyamide nanofiltration membrane with enhanced performance for desalination, Journal of Membrane Science, 523 (2017) 273-281.
[39] W. Gai, X. Li, J.Y. Xiong, C.F. Wan, T.-S. Chung, Evolution of micro-deformation in inner-selective thin film composite hollow fiber membranes and its implications for osmotic power generation, Journal of Membrane Science, 516 (2016) 104-112.
[40] Y. Li, Y. Zhao, E. Tian, Y. Ren, Preparation and characterization of novel forward osmosis membrane incorporated with sulfonated carbon nanotubes, RSC Advances, 8 (2018) 41032-41039.
[41] M. Tian, R. Wang, K. Goh, Y. Liao, A.G. Fane, Synthesis and characterization of high-performance novel thin film nanocomposite PRO membranes with tiered nanofiber support reinforced by functionalized carbon nanotubes, Journal of Membrane Science, 486 (2015) 151-160.
[42] H. Yang, H. Wu, F. Pan, Z. Li, H. Ding, G. Liu, Z. Jiang, P. Zhang, X. Cao, B. Wang, Highly water-permeable and stable hybrid membrane with asymmetric covalent organic framework distribution, Journal of Membrane Science, 520 (2016) 583-595.